

Constraining axion-like particles from rare pion decays

Wolfgang Altmannshofer,^{1,*} Stefania Gori,^{1,†} and Dean J. Robinson^{2,1,‡}

¹*Santa Cruz Institute for Particle Physics, University of California, Santa Cruz, CA 95064, USA*

²*Ernest Orlando Lawrence Berkeley National Laboratory, University of California, Berkeley, CA 94720, USA*

Ultraviolet completions for axion-like particles (ALPs) lighter than the neutral pion generically induce ALP-neutral pion mixing, and are therefore sensitive to direct constraints on the mixing angle. For ALPs below the pion mass, we demonstrate that strong and novel bounds on the ALP-pion mixing angle can be extracted from existing rare pion decay data, measured by the PIENU and PIBETA experiments.

INTRODUCTION

Searches for axion-like particles (ALPs) are a powerful means to probe various extensions of the Standard Model (SM), including models of dark matter, baryogenesis, and solutions to the strong CP problem (see e.g. [1–4]). In the MeV to GeV mass range, the strongest known constraints on such particles arise mainly through their coupling to photons. At large couplings, LEP bounds are applicable from diphoton searches. For a range of somewhat smaller couplings, bounds from beam-dump and fixed-target experiments, such as Charm/Nu-Cal, E137, and E141 apply. Future or current experiments, such as NA62, SeaQuest, and Belle II will probe some of the yet unexplored mass–coupling parameter space.

The phenomenology of an ALP, a , in this mass range may, however, be re-parametrized in terms of its mixing with light unflavored hadrons. The generic nature of this mixing makes it an attractive phenomenological quantity to explore. In particular, UV completions for such ALPs will typically generate ALP-pion mixing, and are therefore sensitive to mixing constraints. In this paper, we demonstrate how strong additional bounds on ALP-pion mixing can be extracted from existing rare pion decay data. We derive these bounds for the mass range $10 \text{ MeV} \lesssim m_a < m_\pi$, extendible down to the massless limit with improved form factor treatments.

Charged pion decays are a promising avenue for ALP searches: The high precision measurements of the chirally-suppressed $\pi^+ \rightarrow e\nu$ (“ π_{e2} ”) and of the phase-space suppressed $\pi^+ \rightarrow \pi^0 e\nu$ (“ π_β ”) branching ratios can place strong constraints on $\text{Br}[\pi^+ \rightarrow a e\nu]$, because the latter has neither of these suppressions. Because any process producing a π^0 in the final state will also produce an ALP in the final state via mixing, these constraints can in turn be transformed into bounds on ALP-pion mixing by estimating the $\pi^+ \rightarrow a e\nu$ amplitude from its mixing with $\pi^+ \rightarrow \pi^0 e\nu$ (cf. Refs. [5, 6]).

The PIENU experiment [7, 8] currently provides the highest precision measurement of the $\pi^+ \rightarrow e\nu$ branching ratio from decays of stopped charged pions: The world average $\text{Br}[\pi^+ \rightarrow e\nu] = (1.230 \pm 0.004) \times 10^{-4}$ [9]. A multicomponent background plus signal fit to the measured positron energy spectra has been used in previous stud-

ies to tightly constrain contributions from heavy sterile neutrinos decays, i.e. $\pi^+ \rightarrow eN$ [7, 10] (see also [11]), and a similar approach has been used for constraining Majoron-neutrino couplings [12]. In this paper, we derive ALP-pion mixing constraints from the PIENU spectra via a similar analysis, leveraging the observation that the irreducible background from $\text{Br}[\pi^+ \rightarrow \pi^0 e\nu]$ is much smaller than the experimental precision. (This is not the case for e.g. $K \rightarrow \pi e\nu$ versus $K \rightarrow e\nu$, for which reason we do not study bounds from semileptonic kaon decays.)

Further, the PIBETA experiment [13] provides the highest precision measurement of the rare $\pi^+ \rightarrow \pi^0 e\nu$ decay, $\text{Br}[\pi^+ \rightarrow \pi^0 e\nu] = (1.036 \pm 0.006) \times 10^{-8}$, including a measurement of the opening angle spectrum of the daughter $\pi^0 \rightarrow \gamma\gamma$ process. This spectrum has a kinematic edge that is highly sensitive to the $\gamma\gamma$ invariant mass. We show that it generates even tighter constraints on $\text{Br}[\pi^+ \rightarrow (a \rightarrow \gamma\gamma) e\nu]$ for a small m_a range.

Previous analyses have considered bounds on ALP-pion mixing using constraints on $K^+ \rightarrow \pi^+ + \text{invisible}$ and estimating the $K^+ \rightarrow \pi^+ a$ amplitude from mixing with $K^+ \rightarrow \pi^+ \pi^0$ (see e.g. Ref. [14]). While powerful, these bounds implicitly require suppression of the ALP-top quark coupling, which can otherwise generate large short-distance $s \rightarrow d$ penguin contributions. E.g. in the case of universal ALP-quark coupling, the penguins are enhanced by $\frac{m_t^4}{32\pi^4 f_\pi^4} \frac{m_a^4}{m_a^4} \frac{|V_{ts} V_{td}|^2}{|V_{us} V_{ud}|^2} \log^2 \left[\frac{m_W^2}{m_t^2} \right]$ compared to the mixing amplitudes [6, 15–17], and naively dominate the $K^+ \rightarrow \pi^+ a$ amplitudes. By contrast, the semileptonic processes we consider arise from tree-level charged-current amplitudes. Short-distance contributions are expected to enter only at higher loop and electroweak order, far smaller than the hadron mixing contributions we probe. In the context of UV completions, the bounds we derive are therefore independent from kaon bounds.

ALP-PION MIXING

The framework we are considering consists of an ALP, a , coupled to SM quarks or gauge bosons, with mass below the pion mass, $m_a < m_\pi$. We assume no tree-level ALP-lepton couplings, and consider only the case that the branching ratio to diphotons is dominant.

The hadronic $\pi^+ \rightarrow \pi^{*0}$ matrix element may be represented by form factors, defined (for SM currents) via

$$\langle \pi^{*0} | \bar{d} \gamma^\mu u | \pi^+ \rangle = c_\pi \left[f_+(p_+^\mu + p_0^\mu) + (f_0 - f_+) \frac{m_+^2 - m_0^2}{q^2} q^\mu \right],$$

in which $q = p_+ - p_0$, the difference of the charged and neutral pseudoscalar momenta, with masses m_+ and m_0 , respectively. We have defined dimensionless form factors $f_{+,0} = f_{+,0}(q^2)$, such that f_0 couples only to the lepton mass. Here $c_\pi = 2 \times 1/\sqrt{2}$ is a coupling combinatoric factor multiplied by a Clebsch-Gordan coefficient. (For $K^+ \rightarrow \pi^0 e \nu$, $c_K = 1/\sqrt{2}$.) The $\pi^+ \rightarrow \pi^{*0} e \nu$ rate

$$\frac{d\Gamma}{dq^2} = \frac{G_F^2 |V_{ud}|^2 c_\pi^2 m_+^3}{24\pi^3} \left(\frac{q^2 - m_e^2}{q^2} \right)^2 r \sqrt{w^2 - 1} \quad (7)$$

$$\times \left[f_+^2 r^2 (w^2 - 1) \left(1 + \frac{m_e^2}{2q^2} \right) + \frac{3m_e^2}{8q^2} f_0^2 (1 - r^2)^2 \right],$$

in which $r = m_0/m_+$, the recoil parameter $w = (m_+^2 + m_0^2 - q^2)/(2m_+m_0)$, with range $1 \leq w \leq (m_+^2 + m_0^2 - m_e^2)/(2m_+m_0)$, and where we have neglected small electroweak corrections [19]. In the regime $m_+ - m_0 \gg m_e$, the electron mass terms may be neglected.

Following from the Ademollo-Gatto theorem [21–23], one expects that $f_+(q^2 = 0) \simeq 1$ up to corrections that are expected to scale as $\sim (m_+^2 - m_0^2)^2/\Lambda_{\text{QCD}}^4$. The matrix element may be expressed as an analytic function of a conformal expansion parameter $z = (\sqrt{w+1} - \sqrt{2})/(\sqrt{w+1} + \sqrt{2})$ [24], so that provided $|z| \ll 1$, the form factor should be approximately linear in w or q^2 . In the analogous $K^+ \rightarrow \pi^0 e \nu$ system, $f_+^K(q^2)$ is well-approximated by a linear function from $f(q^2 = 0) \simeq 1$ to $f(q^2 = q_{\text{max}}^2) \sim 1.2$, and $|z|_{\text{max}} \simeq 0.098$. Thus requiring a sufficiently small z , say $|z|_{\text{max}} \lesssim 0.3$ – equivalent to $r \gtrsim 0.1$ or $m_0 \gtrsim 10$ MeV – and approximating

$$f_+(q^2) \simeq 1, \quad (8)$$

should provide a lower bound on f_+ , yielding an $\mathcal{O}(1)$ level conservative estimate for the $\pi^+ \rightarrow a e \nu$ rate. (In the massless positron limit, applying the approximation (8) to Eq. (7) yields a partial width in agreement with e.g. Eq. (1) of Ref. [13] or Eq. (7.12) of Ref. [19] to $\mathcal{O}[(1-r)^8]$.)

Combining Eqs. (6)–(8) with the $\pi^+ \rightarrow l \nu$ partial width, one then obtains the ratio of branching ratios

$$\frac{\text{Br}[\pi^+ \rightarrow a e \nu]}{\text{Br}[\pi^+ \rightarrow l \nu]} \simeq \frac{2}{3\pi^2} \frac{c_\pi^2 m_\pi^4 \sin^2 \vartheta}{f_\pi^2 m_l^2 (1 - m_l^2/m_\pi^2)^2} \times \int_1^{(1+r^2)/2r} r^4 (w^2 - 1)^{3/2} dw. \quad (9)$$

Using Eq. (9), we proceed to set bounds on $\sin \vartheta$ from rare pion decay data. These bounds rely, in part, on fits to the positron energy spectrum in the parent rest frame. At truth level, the positron energy is bounded by $0 \leq E_e \leq m_+(1 - r^2)/2$, and

$$\frac{d\Gamma}{dE_e} = \frac{c_\pi^2 G_F^2 m_+ E_e^2 ((1 - r^2)m_+ - 2E_e)^2}{8\pi^3 (m_+ - 2E_e)}. \quad (10)$$

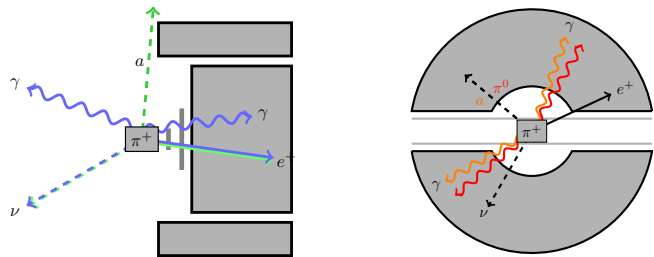


FIG. 1. *Left:* Schematic PIENU detector configuration of the target, tracking and calorimeter elements (gray). Overlaid are typical event topologies for the prompt (decaying to photons, blue) and invisible (green) ALP scenarios. *Right:* Schematic cross-section of the PIBETA detector configuration including the target, tracking and calorimeter elements (gray). Overlaid are typical event topologies for the minimum truth-level opening angle configuration of a π^0 (red) and lighter prompt ALP (orange) diphoton decay.

PIENU RESIDUALS BOUND

The PIENU experiment [8] measures the $\pi^+ \rightarrow e \nu$ branching ratio from a sample of stopped pions, by determining the positron yield in the electromagnetic (EM) inclusive decay $\pi^+ \rightarrow e \nu(\gamma)$ compared to the cascade $\pi^+ \rightarrow (\mu \rightarrow e \nu \nu) \nu(\gamma)$. The main experimental components comprise a target, silicon strips and wire chambers for high precision tracking, a positron calorimeter to reconstruct the positron energy, and a semi-hermetic calorimeter array to capture EM showers. The combined calorimeter energy is given by the sum of positron energy and EM showers, $E_{\text{cal}} = E_e + E_{\text{EM}}$. This necessarily also includes contributions from $\pi^+ \rightarrow e \nu \gamma$. A sketch of the PIENU detector configuration is shown on the left in Fig. 1.

The relevant backgrounds include not only the $\pi^+ \rightarrow \mu \rightarrow e$ cascade, but also contributions from pion decays-in-flight, stopped muon decays, and radiative μ decays to energetic photons. Their branching ratios overwhelmingly dominate the signal mode. Timing cuts are used to suppress these large backgrounds compared to the prompt $\pi \rightarrow e \nu(\gamma)$ modes. A simultaneous fit of the timing distributions for both signal and backgrounds then permits measurement of the ratio, $R_{e/\mu} = \Gamma[\pi \rightarrow e \nu(\gamma)]/\Gamma[\pi \rightarrow \mu \nu(\gamma)]$, at the 10^{-3} level, from which the $\pi^+ \rightarrow e \nu$ branching ratio is inferred.

The E_{cal} distribution for the $\pi^+ \rightarrow e \nu$ mode is sharply peaked at $(m_+^2 + m_e^2)/2m_+ \simeq 69.8$ MeV, with an additional low-energy tail arising from EM shower losses. The (timing-cut-suppressed) backgrounds from the $\pi^+ \rightarrow \mu \rightarrow e$ cascade or muon decays-in-flight are, by contrast, smoothly distributed in the low-energy region $E_{\text{cal}} < E_0 \simeq 52$ MeV, the endpoint.

Refs. [7, 10] perform a precision fit of the measured E_{cal} distribution in the low-energy region to the com-

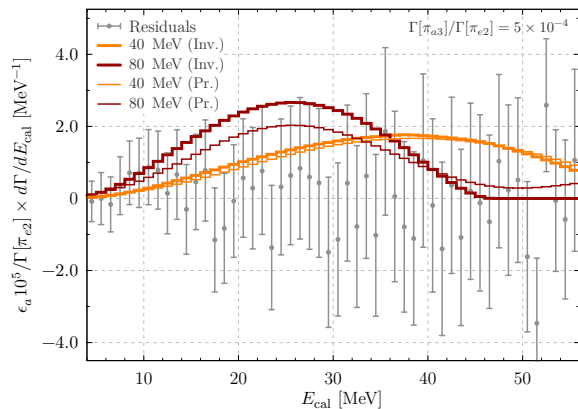


FIG. 2. PIENU fit bin residuals (grey) for the E_{cal} distribution in the low-energy regime, normalized against the $\pi^+ \rightarrow e\nu$ (“ π_{e2} ”) rate. Overlaid are $\pi^+ \rightarrow e\nu$ (“ π_{a3} ”) binned spectra for the prompt (thin solid) and invisible (thick solid) regimes, with $m_a = 40$ MeV (orange) and 80 MeV (red). The spectra include acceptance corrections, with total acceptance ϵ_a , but are normalized such that $\Gamma[\pi_{a3}]/\Gamma[\pi_{e2}] = 5 \times 10^{-4}$.

bin of the (simulated) $\pi^+ \rightarrow e\nu(\gamma)$ low-energy tail and the background distributions. The bin residuals of this fit can be used to place strong constraints on additional prompt contributions from exotic $\pi^+ \rightarrow eX$, where X has sufficient invariant mass to push the *signal* E_{cal} distribution into the low-energy fit region. Refs. [7, 10] consider the case that $X = N$, a heavy sterile neutrino. In Fig. 2 we show the residuals of Ref. [10] used for such an analysis, normalized against the $\pi^+ \rightarrow e\nu$ branching ratio. In this work we consider instead $X = a\nu$, making use of Eq. (9) to convert the bound on branching ratios to a bound on $\sin^2 \vartheta$. (More precise limits will require a dedicated analysis fitting the $X = a\nu$ signal template simultaneously with the background components.)

In the regime that the ALP is long-lived enough to be invisible to the detector, the E_{cal} distribution receives no additional contributions from $a \rightarrow \gamma\gamma$. Overlaid on Fig. 2 we show the corresponding binned positron energy spectra (thick lines) from $\pi^+ \rightarrow ae\nu$ decays for $m_a = 40$ and 80 MeV, including quoted acceptance corrections [10].

In the prompt ALP regime, however, daughter photons of the ALP may contribute to the measured E_{cal} in the event. For $m_a \sim m_\pi$, the ALP is slow enough that one photon may hit the PIENU positron calorimeter within the $\sim 20\%$ positron acceptance [10], as sketched in Fig. 1 (deposition in the outer calorimeters is required to be < 2 MeV [10], thereby excluding hard photon contributions in those). But for $m_a \ll m_\pi$, the ALP momentum may back-react against the lepton system, such that the daughter photons, which decay in a narrow cone around the ALP momentum, miss the acceptance. In Fig. 2 we show the corresponding binned positron spectra (thin lines) for the same two mass benchmarks. The heavier 80 MeV benchmark is slightly altered by a longer tail.

While Ref. [10] does not quote the bin residual correlations, one may reproduce quoted $\pi^+ \rightarrow eN$ bounds assuming nearby bins are uncorrelated. We therefore extend this assumption to treat all bins as uncorrelated over the measured energy range. Under this assumption, in the left panel of Fig. 3 we show the corresponding 95% CL exclusion regions in the $\sin^2 \vartheta - m_a$ parameter space, for both the invisible (green) and prompt (blue) regimes, which are very similar. The excluded regions in $\sin^2 \vartheta$ for the prompt and invisible cases differ at most by $\mathcal{O}(1)$ and extend down to $\sin^2 \vartheta \gtrsim 10^{-5}$. This corresponds to branching ratios as small as $\mathcal{O}(10^{-8})$.

A full study of regimes outside the prompt or invisible limits requires simulation of the PIENU response when the EM shower is somewhat spatially or time-displaced from the prompt decays, but still within the detector acceptance. As a proxy for such a study, we characterize whether the ALP is prompt or invisible by considering whether the mean characteristic ALP displacement from decay-in-flight, $\langle \beta\gamma \rangle c\tau$, is inside the target or outside the calorimeter radius, respectively: We treat the PIENU target size as ~ 1 cm and the calorimeter size as ~ 1 m.

Independent of the relationship between $\sin \vartheta$ and the lifetime (cf. Eq. (3)), requiring a prompt ALP $-\langle \beta\gamma \rangle c\tau < 1$ cm – directly implies a lower bound on $g_{a\gamma}^{\text{eff}}$. Over the ALP mass ranges consider in this paper, we have checked that this bound is far smaller than, and is therefore not saturated by, the direct $g_{a\gamma}^{\text{eff}}$ bounds from LEP tri-photon searches [28, 29]. Electron fixed-target experiments such as NA64 [30] and LDMX [31], as well as Belle(II) [26] and BaBar [32], also have invisible ALP searches. However, for these experiments, the ALP production and lifetime is controlled by $g_{a\gamma}^{\text{eff}}$, independent of $\sin \vartheta$. Hence these constraints do not appear in the left panel of Fig. 3.

The pure mixing regime ($g_{a\gamma} = 0$ in Eq. (3)) fixes the relationship between the $\pi^+ \rightarrow ae\nu$ branching ratio and the ALP lifetime, and may therefore interpolate between the prompt and invisible regimes in different parts of the $\sin^2 \vartheta - m_a$ space. For the pure mixing regime, in Fig. 3 the regions $\langle \beta\gamma \rangle c\tau < 1$ cm (> 1 m) are above (below) the red dot-dashed contours. Above the 1 cm contour, the prompt exclusion should be a good proxy for the mixing regime one. Similarly, below the 1 m contour the invisible regime should well-represent the mixing regime exclusion.

In the mixing regime, one may make use of the relation $g_{a\gamma}^{\text{eff}} \simeq \sin \vartheta g_{\pi\gamma}$ to recast beam-dump, collider, and fixed-target experiment bounds on $g_{a\gamma}^{\text{eff}}$ onto the $\sin^2 \vartheta - m_a$ space. For $m_a < m_\pi$, the relevant bounds are set by the CHARM/Nu-Cal [33–36], E137 [37], E141 [38] and LEP [28, 29] experiments, corresponding in the right panel of Fig. 3 to the regions shaded in gray. As shown in the figure, above the gray regions, we may use the prompt regime exclusion as a proxy for the mixing regime. We see that the PIENU data places powerful new constraints on ALPs *in the mixing regime* for $m_a \gtrsim 25$ MeV.

These constraints will be complemented in the future

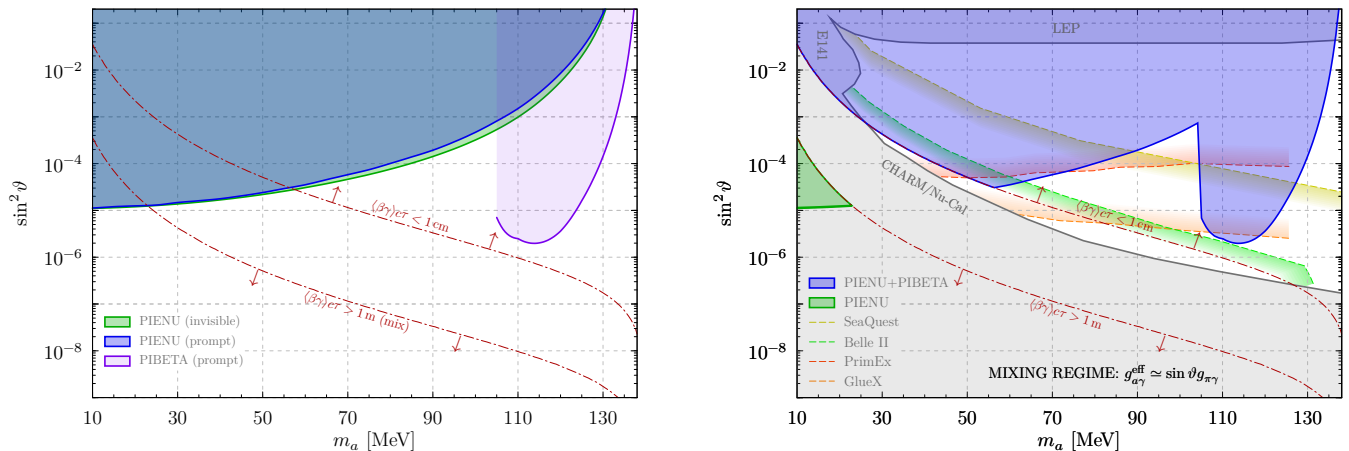


FIG. 3. *Left*: 95% CL exclusion regions from the PIENU fit residuals for the prompt (blue) and invisible (green) ALP regimes. Also shown is the PIBETA exclusion from the $\theta_{\gamma\gamma}$ spectrum for prompt ALPs (purple). *Right*: Combined PIENU and PIBETA exclusion regions for the mixing regime, $g_{a\gamma}^{\text{eff}} \simeq \sin\vartheta g_{\pi\gamma}$. In this regime the mean characteristic decay length regions $\langle\beta\gamma\rangle c\tau < 1\text{ cm}$ (dot-dashed red line and above) and $\langle\beta\gamma\rangle c\tau > 1\text{ m}$ (dot-dashed red line and below) approximately delineate where the prompt and invisible regime exclusions apply, respectively. Also shown are exclusions from CHARM/Nu-Cal, E137, E141 and LEP (grey), and projected reaches for SeaQuest (yellow line and below) [25], Belle II (green line and below) [26], PrimEx (red line and above) and GlueX (orange line and above) [27].

by proton fixed-target beam-dump experiments, such as SeaQuest [25] searching for 3γ signatures or Belle II monophoton searches [26]. In the right panel of Fig. 3, we show the SeaQuest (yellow, 10^{20} protons on target) and Belle II (green) reaches as representatives of experiments capable of setting upper bound limits in the $\sin^2\vartheta$ - m_a parameter space in the pure mixing regime. Part of the $\sin^2\vartheta$ - m_a space may also be tested by NA62 running in beam-dump mode [39], and FASER [40]. A slightly larger region of parameter space will be probed by the SHiP experiment [41]. In a complementary manner, sizable values of the mixing angle $\sin\vartheta$ can be also tested [27] in the future by the PrimEx and GlueX experiments (region above the red and orange lines, respectively).

PIBETA DIPHOTON BOUND

The PIBETA experiment [13, 42] directly measures the rare $\pi^+ \rightarrow (\pi^0 \rightarrow \gamma\gamma)e\nu$ branching ratio, by triggering on the prompt $\pi^0 \rightarrow \gamma\gamma$ decay in coincidence with a positron track from a sample of stopped pions. The main detector elements relevant to this discussion are a near-spherical electromagnetic calorimeter, as well as cylindrical multi-wire proportional tracking chambers surrounded by plastic scintillator. A schematic of the experiment is shown on the right in Fig. 1.

The photon showers are required to each have energy $E_\gamma > m_\mu/2$, beyond the kinematic endpoint of stopped $\mu \rightarrow e\nu\nu$ background decays. The overall normalization of the $\pi^+ \rightarrow \pi^0 e\nu$ rate is obtained via comparison with a large prescaled sample of non-prompt single

positron track events, including both $\pi^+ \rightarrow e\nu$ and in-flight $\mu \rightarrow e\nu\nu$ backgrounds. This comparison entails a simultaneous fit of signal and background kinematic and timing distributions.

Reconstruction of the diphoton pair includes measurement of the diphoton opening angle in the lab frame. At truth level, the diphoton opening angle is bounded via

$$-1 \leq \cos\theta_{\gamma\gamma} \leq -1 + 2\left(\frac{1-r^2}{1+r^2}\right)^2. \quad (11)$$

The maximum (minimum) cosine corresponds to diphoton emission perpendicular (parallel) to the π^+ direction of flight in the π^0 rest frame, generating a sharp kinematic edge (smooth kinematic endpoint) in the $\theta_{\gamma\gamma}$ spectrum. Because the upper bound increases as m_a decreases, the *prompt* diphoton decay of an ALP in $\pi^+ \rightarrow (a \rightarrow \gamma\gamma)e\nu$ with $m_a < m_\pi$ may then produce diphoton showers with truth-level opening angles beyond the π^0 edge at $\sim 176^\circ$. In Fig. 1 we show schematically the maximum truth-level $\cos\theta_{\gamma\gamma}$ configuration for a π^0 compared to a lighter ALP.

In practice, the finite detector-level angular resolution smears out the reconstructed $\theta_{\gamma\gamma}$ distribution and thus the $\theta_{\gamma\gamma}$ edge. Including this effect, for an angular smearing $\sigma_{\theta_{\gamma\gamma}} \simeq 2.25^\circ$ and requiring both photons' energy $E_\gamma > 53\text{ MeV}$ [42], we show in Fig. 4 the expected $\theta_{\gamma\gamma}$ distributions for several m_a benchmarks, as well as for π^0 , compared to the measured $\theta_{\gamma\gamma}$ spectrum in the range $160^\circ \leq \theta_{\gamma\gamma} \leq 180^\circ$ [13]. We see that the π^0 spectrum (grey) agrees well with the data. For $m_a \lesssim 110\text{ MeV}$, the photon energy cut significantly suppresses the $\theta_{\gamma\gamma}$ spectrum in the 160 – 180° range.

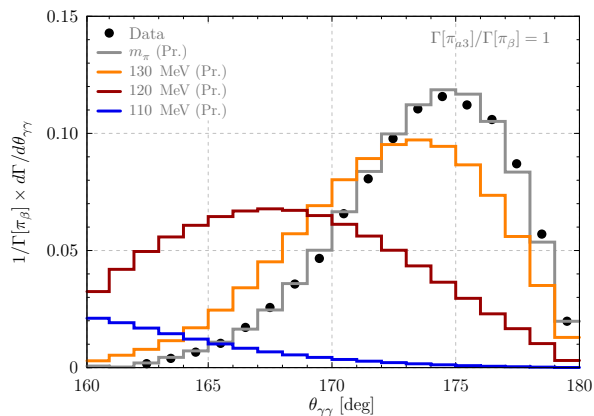


FIG. 4. PIBETA reconstructed diphoton opening angle distribution (black) for $\pi^+ \rightarrow (\pi^0 \rightarrow \gamma\gamma)e\nu$, normalized to unity. Also shown are $\pi^+ \rightarrow ae\nu$ binned spectra for the prompt regime, with $m_a = 110, 120, 130$ MeV and m_π . The spectra are normalized such that $\Gamma[\pi^+ \rightarrow ae\nu]/\Gamma[\pi^+ \rightarrow \pi^0 e\nu] = 1$.

The PIBETA experiment does not provide residuals for the fit of the simulated $\pi^+ \rightarrow \pi^0 e\nu$ opening angle spectrum to the data. Instead, we can extract an approximate, estimated bound on $\sin^2 \vartheta$, by conservatively requiring that the integrated contribution to the $\theta_{\gamma\gamma}$ spectrum in the 160–180° range from $\pi^+ \rightarrow ae\nu$ not exceed the quoted 0.6% uncertainty for the $\pi^+ \rightarrow \pi^0 e\nu$ branching ratio. In Fig. 3 we show the corresponding exclusion (see purple region on the left panel). This exclusion will likely be much stronger if the full differential information shown in Fig. 4 can be incorporated. This approximate bound from PIBETA data sets the most stringent bound on the mixing angle $\sin \vartheta$ for prompt regime ALPs with masses above ~ 100 MeV. A future analysis of data for $\theta_{\gamma\gamma} < 160^\circ$ could lead to stringent constraints for a broader range of ALP masses below 100 MeV.

CONCLUSIONS AND OUTLOOK

Models for axion-like-particles (ALPs) generically predict a mixing between the ALP and the SM neutral pion. In this paper we have derived strong new constraints on ALP-pion mixing, by extracting direct constraints on the $\pi^+ \rightarrow ae\nu$ branching ratio from the rare pion decay data measured by the PIENU and PIBETA experiments.

In the pure mixing regime, these constraints complement existing exclusions as well as the reaches of future planned experiments, leading to near complete coverage of the $\sin^2 \vartheta$ – m_a space over many decades of the mixing angle for $10\text{MeV} \lesssim m_a \lesssim m_\pi$. Beyond this regime, the constraints provide exclusions for the very wide range of UV ALP models that generate ALP-pion mixing. Because they arise from charged current tree-level processes, these exclusions can probe UV models that are charac-

teristically different from those probed by similar bounds extracted from $K^+ \rightarrow \pi^+ + \text{invisible}$ decays.

Our approximate treatments of the detector responses can be improved by dedicated ALP analyses in future $\pi^+ \rightarrow e\nu$ or $\pi^+ \rightarrow \pi^0 e\nu$ measurements, that account for e.g. bin correlations, effects of displaced ALP decays, and/or make use of other differential information. Our results also rely on theoretical approximations, expected to introduce no more than $\mathcal{O}(10\%)$ uncertainties, that may be improved with more detailed treatments of the $\pi^+ \rightarrow \pi^* e\nu$ form factors. This in turn would permit extension of these bounds to even lower ALP masses, below ~ 10 MeV.

ACKNOWLEDGEMENTS

We thank Ketevi Assamagan and Emil Frlez for consultations about the PIBETA experiment and Doug Bryman for consultations about the PIENU experiment. We thank Bob Cahn, Zoltan Ligeti, Michele Papucci and Mike Williams for helpful discussions. The research of WA is supported by the National Science Foundation under Grant No. NSF 1912719. The research of SG is supported by the National Science Foundation under the CAREER grant PHY-1915852. The work of DR is supported by the U.S. Department of Energy under contract DE-AC02-05CH11231, and was supported in part by the National Science Foundation under Grant No. NSF 1912719. WA and SG would like to thank KITP for hospitality and acknowledge partial support by the National Science Foundation under Grant No. NSF PHY-1748958. SG would like to thank the Aspen Center for Physics, which is supported by National Science Foundation grant PHY-1607611, where this work was completed.

* Electronic address: waltmann@ucsc.edu

† Electronic address: sgori@ucsc.edu

‡ Electronic address: drobinson@lbl.gov

- [1] J. Jaeckel and A. Ringwald, *Ann. Rev. Nucl. Part. Sci.* **60**, 405 (2010), [arXiv:1002.0329 \[hep-ph\]](https://arxiv.org/abs/1002.0329).
- [2] K. S. Jeong, T. H. Jung, and C. S. Shin, (2018), [arXiv:1811.03294 \[hep-ph\]](https://arxiv.org/abs/1811.03294).
- [3] P. Agrawal and K. Howe, *JHEP* **12**, 029 (2018), [arXiv:1710.04213 \[hep-ph\]](https://arxiv.org/abs/1710.04213).
- [4] D. S. M. Alves and N. Weiner, *JHEP* **07**, 092 (2018), [arXiv:1710.03764 \[hep-ph\]](https://arxiv.org/abs/1710.03764).
- [5] L. M. Krauss and M. B. Wise, *Phys. Lett.* **B176**, 483 (1986).
- [6] W. A. Bardeen, R. Peccei, and T. Yanagida, *Nuclear Physics B* **279**, 401 (1987).
- [7] M. Aoki *et al.* (PIENU), *Phys. Rev.* **D84**, 052002 (2011), [arXiv:1106.4055 \[hep-ex\]](https://arxiv.org/abs/1106.4055).
- [8] A. Aguilar-Arevalo *et al.* (PiENu), *Phys. Rev. Lett.* **115**, 071801 (2015), [arXiv:1506.05845 \[hep-ex\]](https://arxiv.org/abs/1506.05845).

- [9] M. Tanabashi *et al.* (Particle Data Group), *Phys. Rev. D* **98**, 030001 (2018).
- [10] A. Aguilar-Arevalo *et al.* (PIENU), *Phys. Rev. D* **97**, 072012 (2018), [arXiv:1712.03275 \[hep-ex\]](#).
- [11] A. Aguilar-Arevalo *et al.* (PIENU), (2019), [arXiv:1904.03269 \[hep-ex\]](#).
- [12] C. E. Picciotto, S. Ahmad, D. I. Britton, D. A. Bryman, E. T. H. Clifford, P. Kitching, Y. Kuno, J. A. Macdonald, T. Numao, A. Olin, J.-M. Poutissou, J. Summhammer, and M. S. Dixit, *Phys. Rev. D* **37**, 1131 (1988).
- [13] D. Pocanic *et al.*, *Phys. Rev. Lett.* **93**, 181803 (2004), [arXiv:hep-ex/0312030 \[hep-ex\]](#).
- [14] F. Björkeröth, E. J. Chun, and S. F. King, *JHEP* **08**, 117 (2018), [arXiv:1806.00660 \[hep-ph\]](#).
- [15] M. B. Wise, *Phys. Lett.* **103B**, 121 (1981).
- [16] J. M. Frere, J. A. M. Vermaseren, and M. B. Gavela, *Phys. Lett.* **103B**, 129 (1981).
- [17] L. J. Hall and M. B. Wise, *Nucl. Phys.* **B187**, 397 (1981).
- [18] M. Bauer, M. Neubert, and A. Thamm, *JHEP* **12**, 044 (2017), [arXiv:1708.00443 \[hep-ph\]](#).
- [19] A. Sirlin, *Rev. Mod. Phys.* **50**, 573 (1978).
- [20] T. Cowan, H. Backe, K. Bethge, H. Bokemeyer, H. Folger, J. S. Greenberg, K. Sakaguchi, D. Schwalm, J. Schweppe, K. E. Stiebing, and P. Vincent, *Phys. Rev. Lett.* **56**, 444 (1986).
- [21] R. E. Behrends and A. Sirlin, *Phys. Rev. Lett.* **4**, 186 (1960).
- [22] M. Ademollo and R. Gatto, *Phys. Rev. Lett.* **13**, 264 (1964).
- [23] H. Leutwyler and M. Roos, *Zeitschrift für Physik C Particles and Fields* **25**, 91 (1984).
- [24] C. Bourrely, B. Machet, and E. de Rafael, *Nuclear Physics B* **189**, 157 (1981).
- [25] A. Berlin, S. Gori, P. Schuster, and N. Toro, *Phys. Rev. D* **98**, 035011 (2018), [arXiv:1804.00661 \[hep-ph\]](#).
- [26] M. J. Dolan, T. Ferber, C. Hearty, F. Kahlhoefer, and K. Schmidt-Hoberg, *JHEP* **12**, 094 (2017), [arXiv:1709.00009 \[hep-ph\]](#).
- [27] D. Aloni, C. Fanelli, Y. Soreq, and M. Williams, (2019), [arXiv:1903.03586 \[hep-ph\]](#).
- [28] *JHEP* **06**, 173 (2015), [arXiv:1409.4792 \[hep-ph\]](#).
- [29] J. Jaeckel and M. Spannowsky, *Phys. Lett.* **B753**, 482 (2016), [arXiv:1509.00476 \[hep-ph\]](#).
- [30] D. Banerjee *et al.* (NA64), *Phys. Rev. D* **97**, 072002 (2018), [arXiv:1710.00971 \[hep-ex\]](#).
- [31] (2018), [arXiv:1808.05219 \[hep-ex\]](#).
- [32] P. del Amo Sanchez *et al.* (BaBar), *Phys. Rev. Lett.* **107**, 021804 (2011), [arXiv:1007.4646 \[hep-ex\]](#).
- [33] F. Bergsma *et al.* (CHARM), *Phys. Lett.* **157B**, 458 (1985).
- [34] J. Blumlein *et al.*, *Z. Phys.* **C51**, 341 (1991).
- [35] J. Blumlein *et al.*, *Int. J. Mod. Phys.* **A7**, 3835 (1992).
- [36] *JHEP* **02**, 018 (2016), [JHEP02,018(2016)], [arXiv:1512.03069 \[hep-ph\]](#).
- [37] J. D. Bjorken, S. Ecklund, W. R. Nelson, A. Abashian, C. Church, B. Lu, L. W. Mo, T. A. Nunamaker, and P. Rassmann, *Phys. Rev. D* **38**, 3375 (1988).
- [38] *Proceedings of the PHOTON-2017 Conference: CERN, Geneva, Switzerland, May 22-26, 2017*, *CERN Proc.* **1**, 253 (2018), [arXiv:1708.05776 \[hep-ph\]](#).
- [39] J. Beacham *et al.*, (2019), [arXiv:1901.09966 \[hep-ex\]](#).
- [40] J. L. Feng, I. Galon, F. Kling, and S. Trojanowski, *Phys. Rev. D* **98**, 055021 (2018), [arXiv:1806.02348 \[hep-ph\]](#).
- [41] S. Alekhin *et al.*, *Rept. Prog. Phys.* **79**, 124201 (2016), [arXiv:1504.04855 \[hep-ph\]](#).
- [42] E. Frlez *et al.*, *Nucl. Instrum. Meth.* **A526**, 300 (2004), [arXiv:hep-ex/0312017 \[hep-ex\]](#).